3-24-2006

Cross-Shore Variation of Wind-Driven Flows on the Inner Shelf in Long Bay, South Carolina, United States

Benjamin T. Gutierrez
University of South Carolina - Columbia

George Voulgaris
University of South Carolina - Columbia, gvoulgaris@geol.sc.edu

Paul A. Work
Georgia Institute of Technology - Main Campus

Publication Info

Published in *Journal of Geophysical Research*, Volume 111, Issue C03015, 2006, pages 1-16.
Gutierrez, B. T., Voulgaris, G., & Work, P. A. (2006). Cross-shore variation of wind-driven flows on the inner shelf in Long Bay, South Carolina, United States. *Journal of Geophysical Research, 111* (C03015), 1-16.

Cross-shore variation of wind-driven flows on the inner shelf in Long Bay, South Carolina, United States

Benjamin T. Gutierrez,[1] George Voulgaris,[2] and Paul A. Work[3]

Received 23 June 2005; revised 21 September 2005; accepted 21 November 2005; published 24 March 2006.

[1] The cross-shore structure of subtidal flows on the inner shelf (7 to 12 m water depth) of Long Bay, South Carolina, a concave-shaped bay, is examined through the analysis of nearly 80 days of near-bed (1.7–2.2 m above bottom) current observations acquired during the spring and fall of 2001. In the spring and under northeastward winds (upwelling favorable) a two-layered flow was observed at depths greater than 10 m, while closer to the shore the currents were aligned with the wind. The two-layered flow is attributed to the presence of stratification, which has been observed under similar conditions in the South Atlantic Bight. When the wind stress was southwestward (downwelling favorable) and exceeded 0.1 N/m^2, vertical mixing occurred, the two-layered flow pattern disappeared, and currents were directed alongshore with the wind at all sites and throughout the water column. In the fall, near-bed flows close to the shore (water depth <7 m) were often reduced compared to or opposed those measured farther offshore under southwestward winds. A simplified analysis of the depth-averaged, alongshore momentum balance illustrates that the alongshore pressure gradient approached or exceeded the magnitude of the alongshore wind stress at the same time that the nearshore alongshore current opposed the wind stress and alongshore currents farther offshore. In addition, the analysis suggests that the wind stress is reduced closer to shore so that the alongshore pressure gradient is large enough to drive the flow against the wind.

Citation: Gutierrez, B. T., G. Voulgaris, and P. A. Work (2006), Cross-shore variation of wind-driven flows on the inner shelf in Long Bay, South Carolina, United States, *J. Geophys. Res.*, *111*, C03015, doi:10.1029/2005JC003121.

1. Introduction

[2] Wind stress is the primary mechanism forcing subtidal currents on the inner shelf. The response to the wind stress depends on stratification and variations in seabed and coastline morphology which can cause spatial and temporal variations in the strength of both alongshore and cross-shore flows [*Chen et al.*, 1999; *Lentz*, 2001; *Gan and Allen*, 2002a, 2002b]. In the presence of stratification, cross-shore-directed flows can occur in distinct surface and bottom layers over the inner shelf even at depths smaller than the Ekman depth [e.g., *Lentz*, 2001; *Austin and Lentz*, 2002]. In addition, variations in coastline morphology and seabed topography influence the velocity field through the conservation of potential vorticity [*Kohut et al.*, 2004], enhanced drag [*Chant et al.*, 2004], or through the development of pressure gradients near coastal capes [*Gan and Allen*, 2002b] or other protruding morphological features [*McNinch and Luettich*, 2000].

[3] Investigations of shelf circulation the South Atlantic Bight (SAB) have focused primarily on the large-scale shelf response to wind and buoyancy forcing as well as the influence of the Gulf Stream (see *Blanton and Atkinson* [1983], *Lee and Atkinson* [1983], *Lee et al.* [1989], review by *Atkison and Menzel* [1985], *Pietrafesa et al.* [1985], *Lee et al.* [1985], and *Boicourt et al.* [1998]). These studies were based mainly on measurements acquired from mid and outer shelf locations whereas the inner shelf was observed with relatively few current meters. The few SAB inner shelf studies that included more thorough inner shelf measurements were located in the Georgia Bight where freshwater discharge from coastal rivers and estuaries is important. These studies found that the local wind forcing and buoyancy are the most influential factors controlling inner shelf dynamics in the SAB [e.g., *Boicourt et al.*, 1998]. Observations have indicated that a freshwater frontal zone can persist within 10–20 km of the coast for most of the year. The resulting density gradient forms a dynamic barrier influencing the transport of low-salinity water from the inner shelf farther offshore [*Blanton*, 1981; *Atkinson et al.*, 1983; *Blanton and Atkinson*, 1983]. During southwestward winds, the low-salinity zone is well formed along the coast, while under northward wind conditions, surface waters are transported across the shelf ejecting low-salinity water from nearshore regions and replacing it with higher-salinity midshelf water from below.

[1]Department of Geological Sciences, University of South Carolina, Columbia, South Carolina, USA.
[2]Marine Science Program, University of South Carolina, Columbia, South Carolina, USA.
[3]School of Civil and Environmental Engineering, Georgia Institute of Technology, Savannah, Georgia, USA.

0148-0227/06/2005JC003121

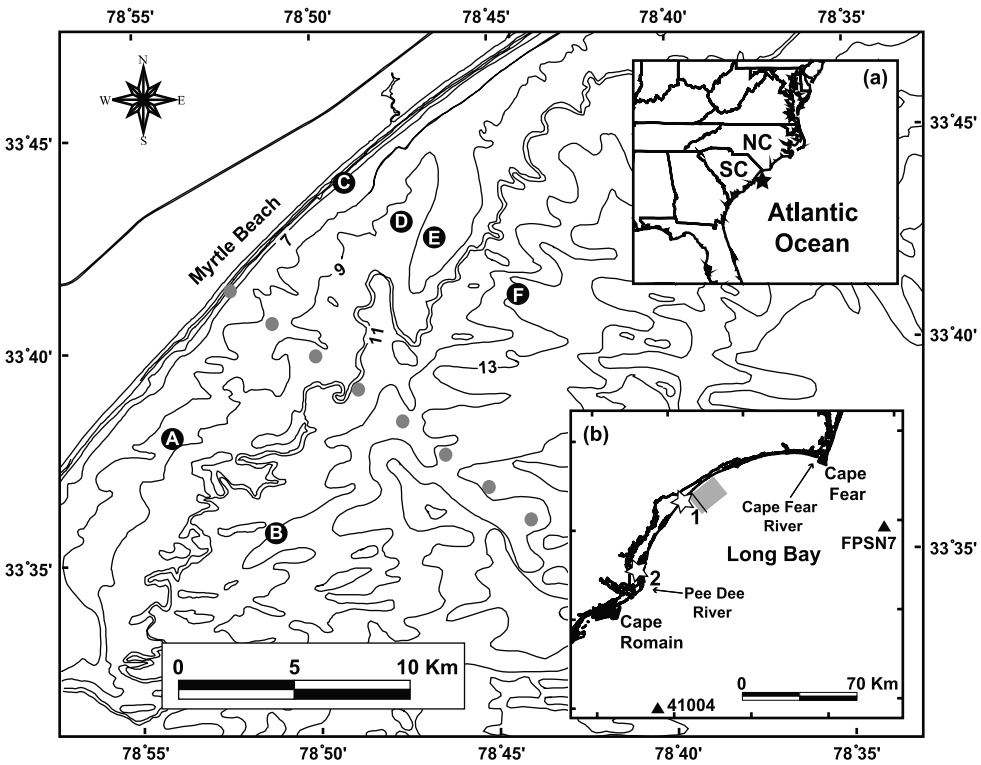

Figure 1. Location map for Long Bay, South Carolina. Instruments were placed at sites A and B during the spring of 2001 and at sites C, D, E, and F during the fall of 2001 (circled letters). Inset map in the top right (labeled a) shows U.S. southeastern seaboard. Inset map in the lower right (labeled b) shows the cuspate shape of the Long Bay coast as well as the NOAA tide gauge stations (stars numbered 1 for Springmaid Pier and 2 for Oyster Landing in inset b) and weather stations (triangles). The shaded area in inset b outlines the study area. Shaded circles denote locations of conductivity-temperature-depth (CTD) stations sampled (also noted by line in inset b) in 2004 for profiles shown in Figure 9. Arrows indicate where Cape Fear and Pee Dee Rivers flow into the South Atlantic Bight. Bathymetry contour interval is 1 m.

[4] Up to this point, studies documenting spatial variation of inner shelf circulation within the SAB have been limited to the Georgia Bight [*Kundu et al.*, 1981] and the remaining current observations used to characterize SAB inner shelf currents have been limited to one or two current meters [*Schwing et al.*, 1983; *Lee et al.*, 1989]. *Schwing et al.* [1983] examined summertime circulation offshore of southern Long Bay near North Inlet, South Carolina (Figure 1), and suggested that the buoyancy dynamics identified along the Georgia Bight inner shelf are not as important for the inner shelf of the northern portion of the South Carolina. This portion of the SAB, called the Grand Strand, is one of the most highly visited stretches of coast in the United States (Figure 1), and is often faced with environmental problems related to beach contamination by bacteria following storm water discharge that lead to occasional beach closings [*Van Dolah*, 2003]. In addition hypoxia in nearshore waters, similar to that noted off the New Jersey coast [*Glenn et al.*, 1996], is facilitated by the affect of stratification on the circulation in response to northeastward winds. As such, spatial flow variations that are altered by stratification [e.g., *Wong*, 1999; *Lentz*, 2001] and/or bathymetric variations [e.g., *Kohut et al.*, 2004; *Chant et al.*, 2004] can potentially impact nearshore water quality.

[5] In this contribution, a set of near-bed current observations from Long Bay, South Carolina, are evaluated to identify the occurrences and causes of horizontal gradients in subtidal wind driven currents. In particular, we focus on the causes of (1) a two-layered flow pattern that occurred during northeastward winds and (2) a flow reversal that was observed close to the coast during southwestward winds. First, the current data sets that were acquired in the spring and fall of 2001 are presented in section 2. In section 3, the meteorological conditions that prevailed during the measurement periods are described. The horizontal variations in circulation during the spring and fall periods as well as description of specific flow events in the fall are presented in sections 4.1, and 4.2 respectively. In section 4.3, the observed variations in near-bed currents for the fall period are explored using a momentum balance analysis and the results are discussed in section 5.

2. Oceanographic Observations

2.1. Field Study

[6] Current measurements reported in this study were acquired during two observation periods in the mid spring and late fall of 2001. A total of six current meters were arranged along two shore-normal transects located offshore

Table 1. List of Instruments Deployed During the Fall and Spring of 2001[a]

Site	Deployment	Instrument	Water Depth, m	Measurement Height, m above seabed	Depth Cell Range, m above seabed	Vertical Resolution, m	*dt*, s
A	spring	Sontek Argonaut	9.3	1.7	-	1	1800
B	spring	RDI ADCP	12.1	1.7	1.5–10.7	0.25	900
C	fall	Sontek Argonaut	7.0	1.7	-	1	1800
D	fall	Nortek Aquadopp	9.7	1.9	1.4–3.9	0.5	900
E	fall	RDI ADCP	8.4	1.7	1.7–7.2	0.5	900
F	fall	RDI ADCP	12.4	2.2	2.2–10.7	0.5	900

[a]Heights of the near-bed velocity bins that are compared in this study are specified under "Measurement Height."

of the southern portion of Myrtle Beach, South Carolina, in the spring and offshore of North Myrtle Beach, South Carolina, in the fall (Figure 1). During the spring period, (21 April to 31 May 2001), currents and pressure were monitored at two locations 3 and 9 km offshore of southern Myrtle Beach (stations A and B, respectively, see Figure 1). During the fall deployment (10 November 2001 to 15 January 2002) four current meters were deployed along a single transect offshore of North Myrtle Beach (stations C, D, E, and F, see Figure 1). Near-bed currents were measured at sites A, C, and D while currents were measured throughout the water column using acoustic Doppler velocity profilers (ADCP) at sites B, E, and F. Our analysis in this paper focuses mainly on the near-bed currents measured at these locations. Current observations throughout water column are used at site B only to provide a context for observations in section 4.1 during the spring. Detailed information regarding the current meters deployed at each site is provided in Table 1. Also, near-bed salinity, temperature, and pressure data were acquired near the seabed with SeaBird CTDs at sites E and F.

[7] In addition to currents, surface wave data were collected at all sites. These measurements although not discussed in detail in this contribution are used to estimate mean current shear stresses accounting for the combined action of waves and currents [*Styles and Glenn*, 2000] as explained in section 4.3.

2.2. Data Analysis

[8] Owing to differences in sampling schemes (see Table 1) all current records were subsampled at 1-hour intervals so that all velocity observations represent flow conditions at nearly the same time (within 3 min). The current time series were then low-pass filtered to remove variations occurring at periods less than 33 hours [*Beardsley et al.*, 1985]. Prior to analysis, the velocities were rotated into an along/cross-shore orthogonal coordinate system with the positive alongshore (x) axis oriented to the northeast (40°T) and the positive cross-shore axis directed onshore toward the northwest (310°T). In this paper, "near-bed currents" refers to currents measured at heights ranging from 1.7 to 2.2 m above the seabed depending on location (Table 1).

[9] No meteorological data exist at the inner shelf in the study site. The nearest NOAA/National Data Buoy Center weather stations are (1) 50 km offshore of Cape Fear approximately 100 km northeast of the study area (station FPSN7) and (2) 120 km south of the study region (Buoy 41004). Intercomparison of time series from both stations (not shown here) indicated that the data are well correlated which suggests that meteorological characteristics do not vary over the study area. Because data from the station FPSN7 were more complete than those from Buoy 41004, the information from the former station were used to evaluate wind forcing in this study.

[10] Wind speed observations were used to estimate wind shear stress values using a quadratic formula that relates the wind speed at 10 m above the sea surface to a shear stress value through the use of a neutral drag coefficient [*Large and Pond*, 1981]. The observed wind speeds and directions were converted to velocities at 10 m assuming a logarithmic velocity profile with a roughness parameter defined by the drag coefficient. Lastly, the wind shear stress time series was low-pass filtered with the same technique that was used for the current time series.

[11] Freshwater discharge was inferred from U.S. Geological Survey streamflow data for the Cape Fear (station 02105769 at Kelly, North Carolina) and Pee Dee (station 02131010) Rivers, the two major sources of fresh water in the study area.

3. Meteorological Conditions

[12] Sustained periods of northeastward and southwestward wind stress that are nearly aligned with the coastline (40°T) dominated the wind observations. In the spring period, several events occurred where strong northeastward (i.e., upwelling favorable) winds shifted rapidly to southwestward (i.e., downwelling favorable, see Figure 2). These transitions were accompanied commonly by a drop in temperature and pressure and resembled the typical meteorological pattern of low-pressure systems that move across the southeastern United States [e.g., *Austin and Lentz*, 1999]. In the spring period, the southwestward winds occurred for 30% of the time, while the northeastward winds occurred for 44% of the time period. In the fall, southwestward wind conditions dominated a larger portion of the wind stress time series occurring 51% of the time, while only three northeastward wind periods occurred comprising 14% of the observation period. There was one instance where northwestward wind stress persisted for a prolonged period (approximately 30 hours). This accounted for 9.5% of the time during the fall data collection period.

[13] River discharge, which is an indication of freshwater input to the coastal ocean, was relatively low during the study period compared to the previous 4 years in the Cape Fear River and Pee Dee River (Figure 3). The discharge of the Cape Fear River was similar during both experimental periods averaging 33.3 and 32.4 m^3/s for the spring (Figure 3a) and fall (Figure 3b) periods, respectively.

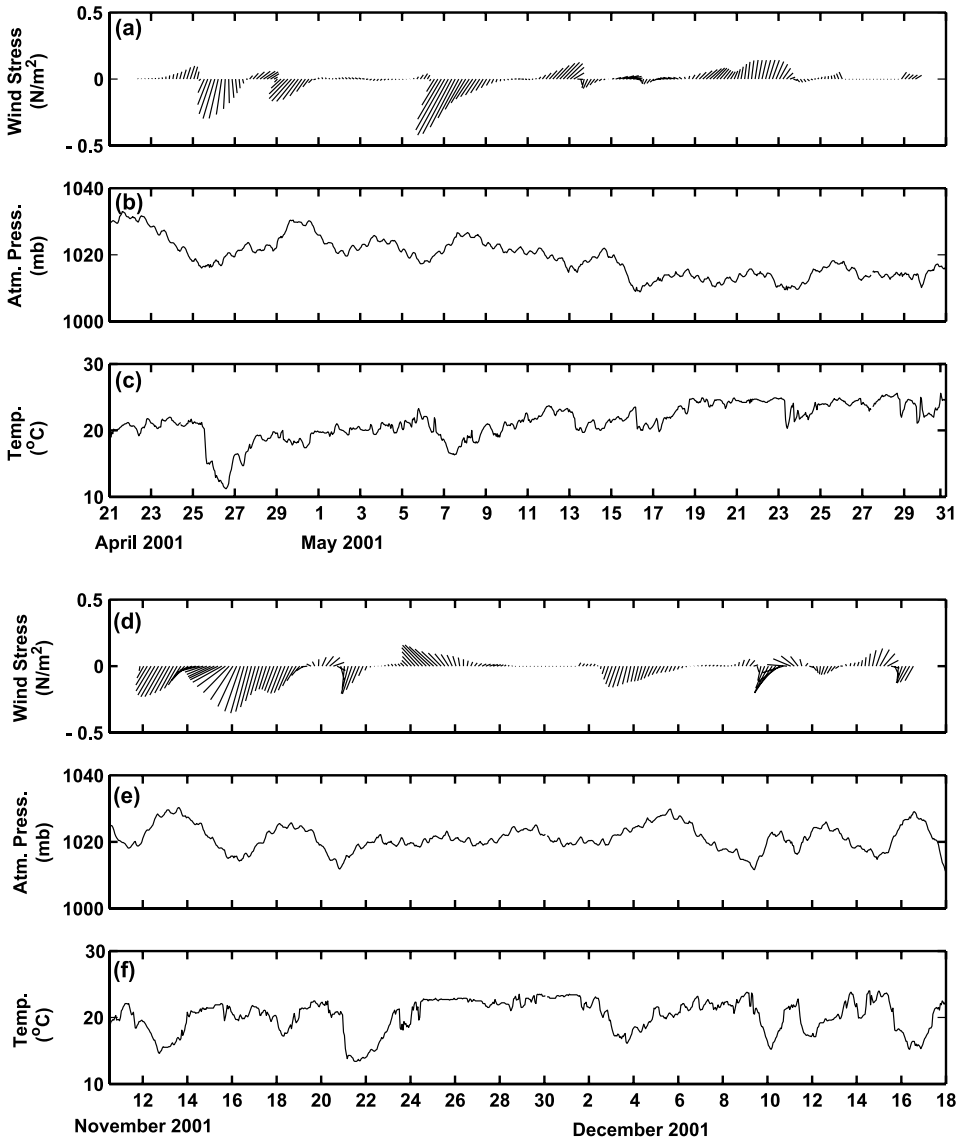

Figure 2. Time series of (a and d) wind stress, (b and e) atmospheric pressure, and (c and f) air temperature from NOAA NDBC weather station at Frying Pan Shoals over the two study periods reported in this paper. In wind stress plots (Figures 2a and 2d) north is oriented toward the top of the page, and the wind directions are displayed in the oceanographic convention.

The flow in the Pee Dee River was consistently near or above 50 m^3/s (mean of 68.7 m^3/s) during the spring, yet during the fall discharge was relatively low (mean discharge was 33.7 m^3/s) surpassing this level only once toward the end of the observation period.

4. Near-Bed Current Observations

[14] This section focuses on the subtidal current variability observed at six inner shelf stations for two different seasons. The statistics from these observation periods are presented in Table 2. It is organized in two parts that present (1) near-bed current observations and their relation to wind forcing for each observation period and (2) a simplified alongshore momentum balance analysis that is used to identify the relative contribution of different forcing terms and their influence on alongshore flows during the fall 2001 period.

4.1. Spring 2001

[15] Near-bed current observations in the spring varied with the alongshore wind stress. Over this period, the principal axes of both the wind stress and near-bed subtidal currents at sites A and B were oriented obliquely to the coast with the major axes oriented 22°–36° clockwise from the coastline (Table 2). Correlations between the alongshore wind stress and near-bed alongshore velocities were found to be 0.77 at site A and 0.68 at site B for a time lag of 2–3 hours (Table 3). In addition, a high correlation ($r = 0.70$ at 99% C.L.) was noted between the alongshore wind stress and the cross-shore current at site B. Between sites A and B, along and cross-shore currents were moderately correlated

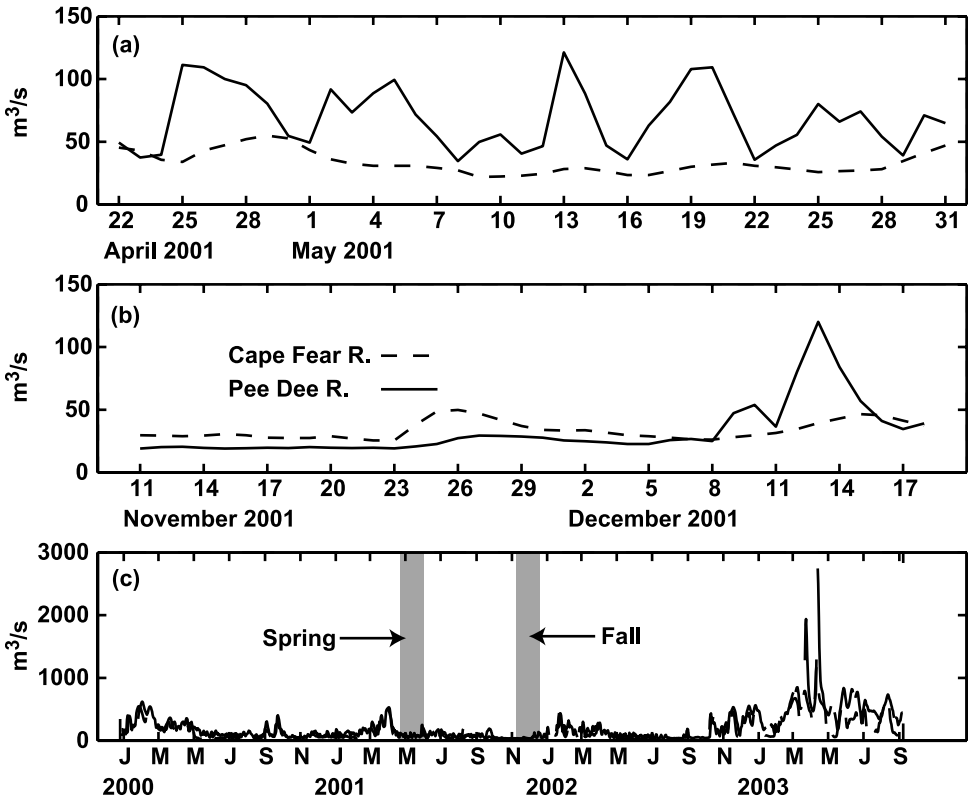

Figure 3. Daily streamflow observations for the Cape Fear and Pee Dee Rivers during the (a) spring and (b) fall of 2001 as well as (c) a 4 year period from 2000 to 2003.

with correlation coefficients of 0.61 and 0.67 (significant at the 99% level), respectively.

[16] In the spring, strong southwestward winds, represented by negative alongshore wind stresses in Figure 4 (events: S2, S4, S6, S8, and S10), coincided with periods where the sea surface was set up as much as 0.3 m above the mean level for the measurement period. At the same time the currents exhibited a typical inner shelf response to southwestward winds (downwelling favorable) with near-bed alongshore currents aligned with the shore and the wind. Three of the distinct southwestward wind events (S2, S4, and S6) were characterized by relatively strong alongshore wind stresses (>0.2 N/m^2) corresponding to near-bed alongshore currents at both sites A and B reaching 0.1 m/s while cross-shelf currents were weaker (0.02–0.05 m/s) and directed offshore. During weaker periods of southwestward wind (events S8 and S10, see Figure 4) the alongshore and cross-shore currents at each site were more equal in magnitude. During event S8, the near-bed flows at site A were stronger than the near-bed current at site B, which exhibited a larger cross-shore flow component (Figure 4). A similar pattern was observed during the initial stages of event S10 where the alongshore current at site B was small and the cross-shore current was larger for both near-bed and depth-averaged currents.

[17] For northeastward winds, which were characterized by positive alongshore wind stresses, the opposite response can be noted. In the spring, the northeastward wind periods

Table 2. Near-Bed Current Statistics for Low-Pass Filtered Current Velocities[a]

	Alongshore Wind/Current				Cross-Shore Wind/Current				Principal Axes		
Location/Depth, m	Mean	SD	Maximum	Minimum	Mean	SD	Maximum	Minimum	Major	Minor	Orientation, deg
					Spring						
Wind (FPSN7)	−0.005	0.1	0.2	−0.5	−0.004	0.05	0.1	−0.2	0.1	0.03	28
Station A/1.7	0.004	0.04	0.1	−0.1	0.01	0.02	0.05	−0.03	0.04	0.02	28
Station B/1.7	−0.01	0.04	0.09	−0.12	0.02	0.03	0.08	−0.06	0.04	0.03	10
					Fall						
Wind (FPSN7)	−0.05	0.1	0.1	−0.3	−0.005	0.07	0.2	−0.2	0.1	0.05	19
Station C/1.7	0.01	0.03	0.06	−0.06	0.003	0.007	0.02	−0.02	0.03	0.01	41
Station D/1.9	−0.001	0.03	0.05	−0.07	0.04	0.01	0.02	−0.03	0.04	0.01	43
Station E/1.7	−0.02	0.03	0.04	−0.11	0.002	0.009	0.02	−0.03	0.03	0.01	226
Station F/2.2	−0.7	0.03	0.05	−0.08	0.002	0.009	0.02	−0.03	0.04	0.01	44

[a]Sensor depths (in m) are noted in parentheses next to the station names. SD is standard deviation. Wind stresses are in units of N/m^2, and currents are in units of m/s. Major axis orientations are referenced to degrees from north.

Table 3. Correlation Coefficients Between Wind Stress and Velocity Components[a]

Station	A	B	C	D	E	F
τ_x	**0.77** **0.53**	**0.68** (**0.85**) **0.70** (**0.67**)	−0.29 −0.05	0.2 *−0.43*	**0.62** (**0.69**) −0.11 (**−0.39**)	**0.51** (**0.58**) −0.14 (**0.65**)
τ_y	**0.58** 0.29	**0.46** (**0.63**) **0.48** (**0.53**)	−0.36 **−0.33**	−0.06 **−0.54**	0.21 (0.29) **−0.31** (−0.22)	0.18 (0.23) *−0.32* (*−0.49*)
A	1	**0.61** **0.67**	-	-	-	-
B		1	-	-	-	-
C			1	**0.54** 0.26	0.17 0.24	0.11 0.25
D				1	**0.86** **0.66**	**0.81** **0.63**
E					1	**0.94** (**0.91**) **0.56** (**0.94**)
F						1

[a]In each cell in Table 3 the correlation coefficient of the alongshore velocities is specified first, and the cross-shore velocity is specified second. Coefficients for depth-averaged values are specified in parentheses. Correlation coefficients that are significant at the 99% level are specified in bold, and those significant to only the 95% level are specified in italics.

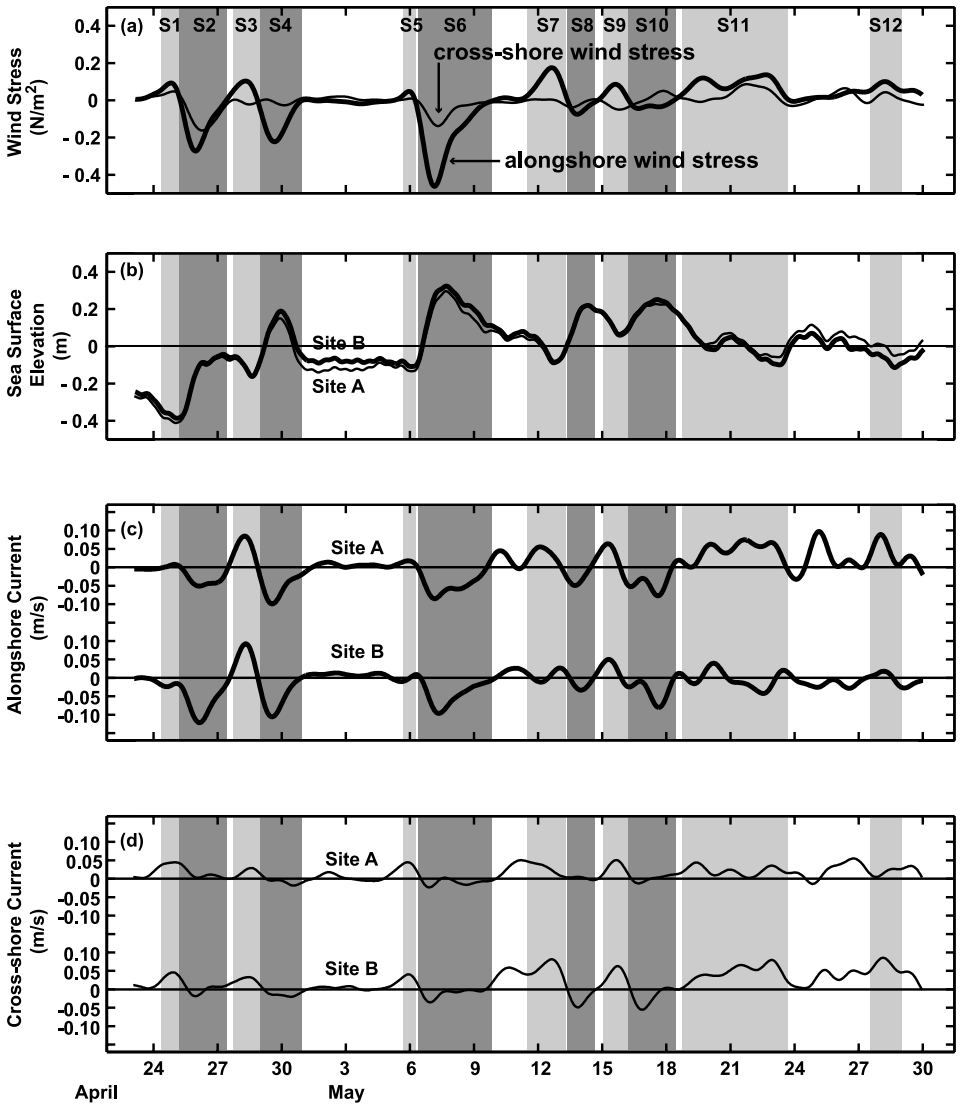

Figure 4. Time series of (a) wind stress vectors, (b) sea surface elevation, (c) alongshore current, and (d) cross-shore current from the spring of 2001 at sites A and B. Upwelling and downwelling wind events are displayed in light and dark gray bands, respectively.

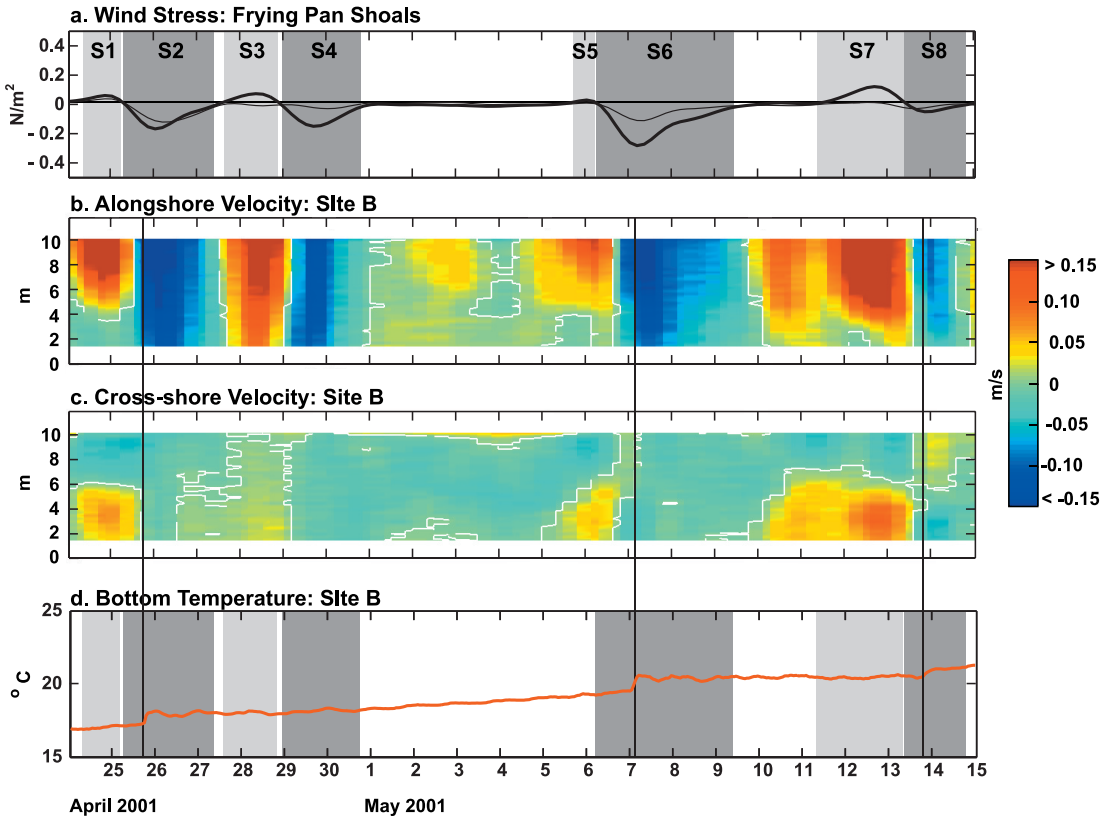

Figure 5. Time series of (a) alongshore and cross-shore wind stress vectors, (b) alongshore current profiles, (c) cross-shore current profiles, and (d) bottom temperature from site B for a 21-day period during the spring. Vertical lines between plots denote increases in bottom temperature that coincide with transitions from upwelling to downwelling favorable wind stresses and the disappearance of two-layered flow in the water column.

were specified as events S1, S3, S5, S7, S9, S11, and S12 (Figure 4). During these times positive alongshore wind stresses coincided with periods of sea level set down reaching 0.4 m below the mean sea level, and strong alongshore currents toward the northeast reaching 0.09 to 0.18 m/s (Figure 4) at site A. In each of these events, with the exceptions of S3 and S9, onshore directed current was noted at site B (see Figure 4, events S1, S5, S7, S11, and S12) while the current site A exhibited a larger alongshore component.

[18] In periods where alongshore currents at sites A and B differed, a two-layered flow pattern (Figure 5, events S1–S8) was observed in the ADCP measurements at site B. This pattern intensified during strong northeastward winds such as those corresponding to events S1, S5, and S7. In these periods, alongshore flows in the surface layer reached 0.15 m/s, while near-bed alongshore flows were relatively weak with velocities less than 0.05 m/s (Figure 5b). In addition, offshore-directed currents in the surface layer reached magnitudes of 0.07 m/s, while in the bottom layer currents were directed onshore ranging from 0.03 to 0.08 m/s (Figure 5c). In event S8, two-layered flow was also observed during a period of relatively weak southwestward wind stress. In this period the alongshore current was relatively weak and a two-layer flow pattern was observed in the cross-shore current profile. Here onshore flows of 0.04 m/s occurred in the surface layer, while near-bed flows were directed offshore reaching 0.05 m/s. It is important to note that the two-layered flow periods that are noted in events S1, S5, and S7 occur during the same periods where near bed cross-shore currents varied between sites A and B (shown previously in Figure 4b).

[19] During southwestward winds, the two-layered flow pattern disappeared when wind stresses exceeded $\sim$0.2 N/m^2 in events S2 and S6 (Figure 5). The first of these transitions occurred at the transition between northeastward (S1) and southwestward winds (S2). Initially during S1, both the alongshore and cross-shore velocity profiles exhibited a two-layered flow pattern. When southwestward wind stresses developed (event S2) and the alongshore wind stress reached -0.13 N/m^2 the two-layered flow disappeared and currents were directed alongshore. Here the alongshore velocities exceeded 0.15 m/s in magnitude while the cross-shore component was less than 0.03 m/s. The disappearance of the two-layered flow coincided with a 0.5°C increase in bottom temperature at site B (Figure 5d). A similar pattern was observed between events S5 and S6. During S5 a two-layer flow pattern developed under northeastward wind conditions. As the negative alongshore wind stress shifted to the southwest, a weak two-layered flow was

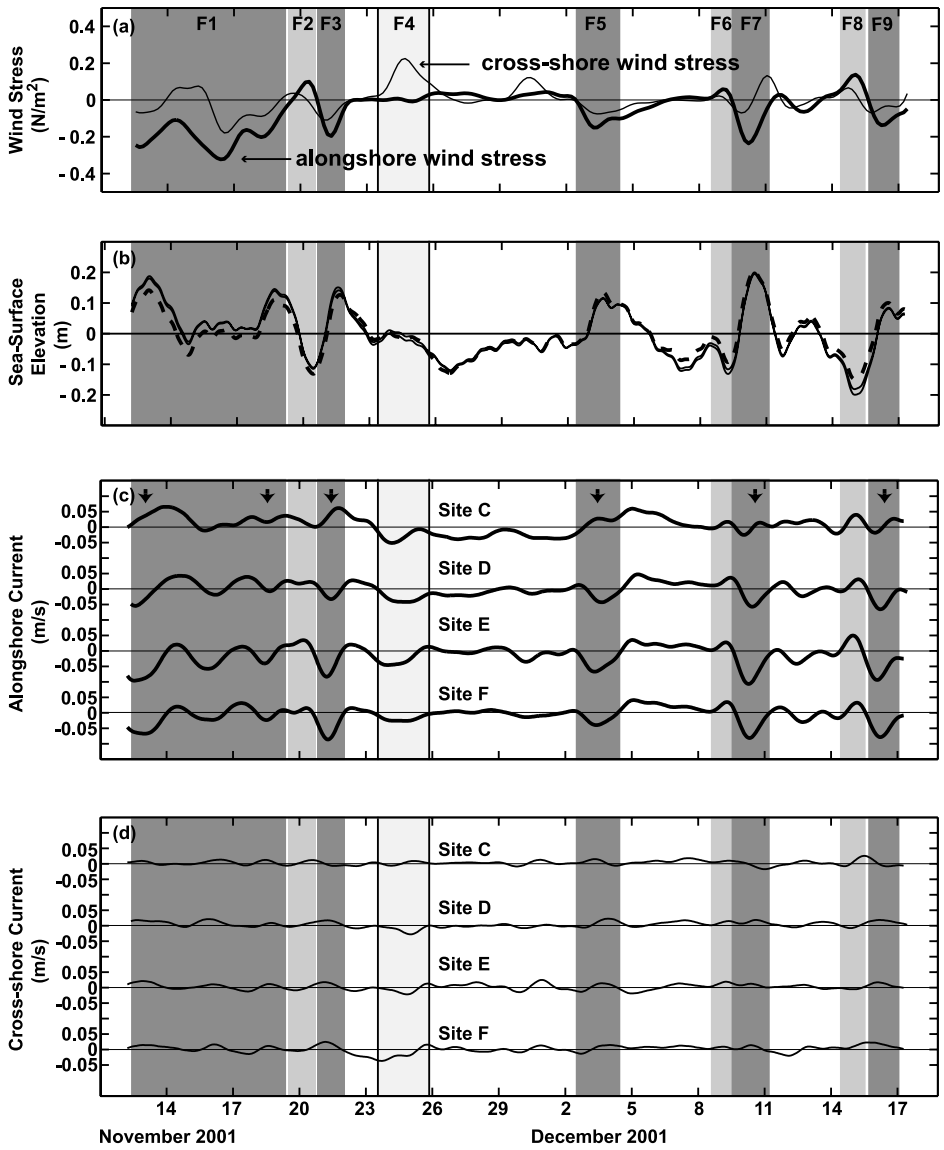

Figure 6. Time series of (a) wind stress vectors, (b) sea surface elevation (site C, dashed line; sites D, E, and F, solid lines), (c) alongshore current, and (d) cross-shore current from the fall of 2001 at sites C, D, E, and F. Upwelling and downwelling wind events are displayed in light and dark gray bands, respectively. Arrows specify periods where alongshore currents at site C are reversed compared to the other stations (Figure 6c).

observed in the cross-shore current profile. When the wind stress reached $\sim$0.3 N/m^2 the two-layered flow was no longer visible and currents were directed alongshore. At the transition between the two-layer and depth uniform flow a 1°C increase in bottom temperature was noted.

4.2. Fall 2001

[20] Time series of alongshore currents show that flows at sites D, E, and F were similar in terms of strength and direction and were well correlated (see Table 3) while those at site C were less coherent particularly during southwestward winds. Principal axes of near-bed currents at sites C, D, E, and F indicate that the subtidal currents were aligned within 1°–10° of the coast (Table 2). In addition the winds stress major axis was oriented within 21° of the coastal orientation. Alongshore currents show that flows at sites D, E, and F are fairly similar in terms of strength and direction and well correlated (r = 0.81–0.94). On the other hand, near-bed alongshore velocities at site C show a moderate correlation (r = 0.54) with alongshore currents at site D and no correlation (r = 0.17 and 0.11) to alongshore components at sites E and F (Table 3). Only the alongshore currents at sites E and F exhibited correlations greater than 0.5 with the alongshore wind stress (Table 3).

[21] Five periods of southwestward wind stress were noted in the fall data set (see events F1, F3, F5, F7, and F9 in Figure 6). During these periods the sea surface set up and the currents were aligned alongshore to the southwest. The exception occurred at site C, where observations show that the alongshore currents at this site were either weaker than those at the other locations or flowed toward the northeast against the wind as well as the currents farther

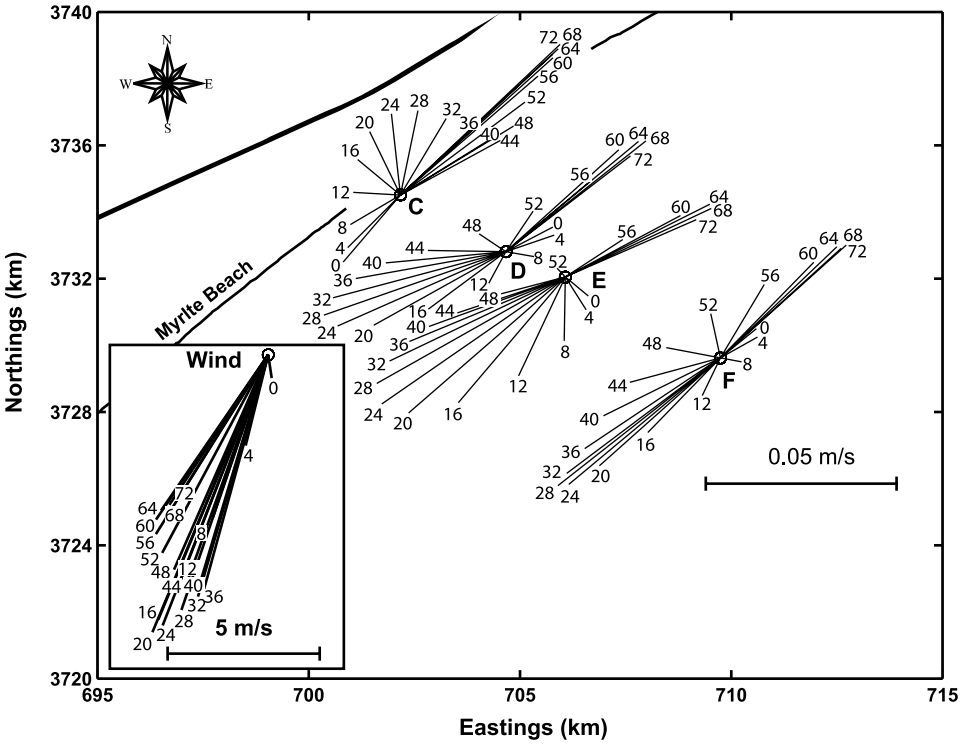

Figure 7. Time series of wind and near-bed currents from sites C–F for the period between 2 December 2001 1200 UT and 5 December 2001 1200 UT. Wind observations are from the NOAA weather station FPSN7 at Frying Pan Shoals. Numbers at the end of wind vectors represent hours since 2 December 1200 UT.

offshore (note arrows in Figure 6). Examples of this are noted during the initial phase and again at the end of event F1 and in events F3 and F5 where the flows at site C oppose those at the other stations. In events F7 and F9 alongshore currents at site C were aligned with the flows measured farther offshore but were also weaker. The observations also revealed that the currents at all four sites reversed direction while southwestward winds diminished (see Figure 6). This phenomenon is discussed in greater detail in below.

[22] Only three distinct upwelling favorable winds persisted during the fall period (Figure 6, events F2, F6, and F8). At these times the northeastward winds resulted in a small depression of the sea surface and a northeastward flowing current. Alongshore currents during these events were comparable yet weak during these conditions (Figure 6, events F2, F6, and F8). Compared to the spring, cross-shore currents were minor during northeastward wind stress possibly because these events occurred for relatively brief periods and were also relatively weak. ADCP observations from both stations E and F during the fall study period did not exhibit the tendency for two-layered flow that was noted in the spring period at site B for similar wind conditions.

4.3. Flow Reversals

[23] As noted in the previous description, two flow patterns were observed prior to and during southwestward wind stresses in the fall. First, the flow at site C opposed or was smaller than that at the other stations during portions of event F1, the full duration of events F3 and F5, and toward the end of event F7 (Figure 6c). In each of these cases the alongshore current at stations D, E, and F was directed toward the southwest (negative sign), while flows at site C were oriented toward the northeast in the opposite direction. Second, during the diminishing stages of the southwestward wind events F3, F5, and F7, near-bed currents at sites D, E, and F rotate from negative (southwestward) to positive (northeastward) alongshore, aligning with flow at site C. This observed flow reversal appears to be similar to upwelling relaxation flows observed on the northwestern coast of the United States [*Winant et al.*, 1987] but instead occurred during downwelling favorable periods in Long Bay.

[24] Both of the phenomena described above can be clearly seen in the data collected over a 72-hour period between 2 December and 5 December (event F5, Figure 7). On 2 December a southwestward wind stress developed and strengthened over a 12-hour period. Over this period the current vectors at sites D, E, and F, which were initially directed to the east and northeast, rotated and aligned with the wind while currents at site C rotated shoreward. As the wind strengthened to its maximum, 20 hours after it began, flows at sites D, E, and F were directed alongshore while flows at site C continued to rotate clockwise. Flows at the offshore sites (D, E, and F) continued to strengthen reaching their maximum between hours 24 and 28. By hour 32 the wind diminished and then rotated slightly to the west. The currents at the offshore sites followed the wind pattern while currents at site C were directed toward the northeast. At hour 44 the currents at the offshore stations decreased and continued to rotate toward the coast. Eight hours later (hour 54 within the event) northeastward currents at site C strengthened and continued to do so until the end of this period. By hour 56, currents at the other stations exhibited

Table 4. Correlation Coefficients for Alongshore Wind Stress, Alongshore Pressure Gradient, and Alongshore Bed Shear Stress During the Fall Observation Period[a]

	$-1/\rho_o$ dP/dx	τ_{bx} (C)	τ_{bx} (D)	τ_{bx} (E)	τ_{bx} (F)
τ_{wx}	**0.75**	−0.3	0.23	**0.74**	**0.62**
$-1/\rho_o$ dP/dx	1	***−0.47***	0.08	**0.5**	**0.41**
		−0.53 (10)			

[a]Results in italics denote correlations that are significant at only the 95% level, and boldface specifies those significant at the 99% level. All correlations were for zero lag except those where lag is noted in parentheses in units of hours.

the same behavior even with the wind blowing in nearly the opposite direction.

4.4. Alongshore Momentum Balance

[25] The alongshore momentum balance was utilized to examine the role of different forcing terms in the observed alongshore current variations during the fall. Ignoring advective acceleration terms and radiation stress terms due to wave breaking, the depth-averaged alongshore momentum balance is

$$\frac{\partial u}{\partial t} - fv = -\frac{1}{\rho_o}\cdot\frac{\partial P}{\partial x} + \frac{\tau_{wx}}{\rho_o H} - \frac{\tau_{bx}}{\rho_o H} \tag{1}$$

where u and v are the depth-averaged alongshore and cross-shore velocity components, respectively, f is the Coriolis coefficient(= 8.07×10^{-5} s^{-1}), P is the water pressure, and τ_{wx} and τ_{bx} are the alongshore wind and bed stresses, respectively. Finally, H is the mean water depth and ρ_o(1026 kg/m^3) is the reference density estimated from the near-bed salinity and temperature observations.

[26] The local acceleration term ($\partial u/\partial t$) was estimated as the centered difference of the raw alongshore velocity values (u) over a 2-hour period. The $\partial u/\partial t$ and $f \cdot v$ terms were calculated only for sites E and F where depth-averaged current measurements were available. The alongshore pressure gradient term ($-1/\rho_o \cdot \partial P/\partial x$) was estimated from the sea surface elevation records from two NOAA tide gauge stations. The first station was located at Springmaid Pier (NOAA station 8662245) 10 km to the south of site C and directly onshore of site A (see Figure 1 inset b). The second station was located within the North Inlet Estuary at Oyster Landing (NOAA station 8661070). Use of hourly observations to estimate the pressure gradient term before applying the low-pass filter, as it was the case for all other terms in equation (2), was not possible. This was because the tidal elevations at the Oyster Landing differ from those in the open ocean because of frictional and nonlinear effects that modify the tidal curve and transfer energy from lower to higher harmonics [e.g., *Aubrey and Speer*, 1984]. Instead the sea surface observations were low-pass filtered prior to calculating the pressure gradient. For the spring period, no pressure measurements were available at the Oyster Landing station and therefore the momentum balance analysis was conducted only for the fall period.

[27] The bottom stress was estimated using the *Styles and Glenn* [2000] benthic boundary layer model (BBLM) to incorporate wave-current interaction that is important in the shallow waters of the inner shelf. This technique was used since the current measurement scheme was not sufficient to directly estimate the bed shear stress through a log profile fit or other method as executed in other inner shelf studies [e.g., *Lentz et al.*, 1999].

[28] At sites E and F, the dominant terms in the momentum balance equation were those related to the wind stress, the pressure gradient, and the bottom stress, which were all on the order of 10^{-6} m/s^2. The Coriolis and acceleration terms were an order of magnitude smaller and will not be considered further. This also implies that the Coriolis and acceleration terms at sites C and D, which could not be estimated, were also small and can be neglected. Correlations between the three largest terms, wind stress, the pressure gradient, and the bottom stress for all four sites are displayed in Table 4.

[29] The largest correlation between the wind stress and bed stress terms (r = 0.74) occurs at site E, while the poorest correlations (r = −0.3 and 0.23) occur at the two stations closest to the shore (C and D). The alongshore pressure gradient term is well correlated with the wind stress (r = 0.75) and shows a moderate correlation (r = −0.47, 0.5 and 0.41) with the bed stress term at sites C, E, and F, respectively but no correlation (r = 0.08) at site D. In addition, the correlation at site C increases from −0.47 to a maximum of −0.53 for a 10-hour time lag.

[30] The alongshore pressure gradient was also estimated between a tidal station on the coast at Cape Hatteras, NC and Oyster Landing which were separated by 270 km (Figure 8). Over this distance, $-1/\rho_o \cdot \partial P/\partial x$ exhibited a positive correlation (R = 0.82) to the $-1/\rho_o \cdot \partial P/\partial x$ estimated within Long Bay. Both alongshore pressure gradients exhibited a similar response during southwestward winds but the $-1/\rho_o \cdot \partial P/\partial x$ estimated over the larger distance was smaller than that computed within Long Bay during 4 out of 5 of the events. In addition, $-1/\rho_o \cdot \partial P/\partial x$ between Cape Hatteras and Oyster Landing was also correlated to the alongshore wind stress from Frying Pan Shoals (R = 0.7).

[31] The time series of the three dominant terms in equation (1) are presented in Figure 8. The comparison of these terms clearly shows that $\tau_{wx}/\rho_o H$ and $-1/\rho_o \cdot \partial P/\partial x$, which make up the largest portion of the alongshore momentum balance, correspond to one another for both upwelling and downwelling favorable periods. In events F1, F5, F7, and F9 periods the relative strength of the $-1/\rho_o \cdot \partial P/\partial x$ approached or exceeded that of the $\tau_{wx}/\rho_o H$ when the flow at site C was reduced compared to or opposed the alongshore flow at site the other sites. In events F1 and F5, the flow at the other locations (D, E, and F) also opposed the wind when $-1/\rho_o \cdot \partial P/\partial x$ exceeded the wind stress. Examination of the offset between peaks in the $\tau_{wx}/\rho_o H$ and $-1/\rho_o \cdot \partial P/\partial x$ in Figure 8 show that the lag between the maximum wind stress and the pressure gradient ranges between 7 and 17 hours for events F3, F5, F7, and F9. This comparison of $-1/\rho_o \cdot \partial P/\partial x$ relative to $\tau_{wx}/\rho_o H$ during these events suggests qualitatively that the relative strength of the two terms influences the alongshore current at this location.

5. Discussion

[32] Spatial gradients in both alongshore and cross-shore currents occurred under both northeastward winds (upwell-

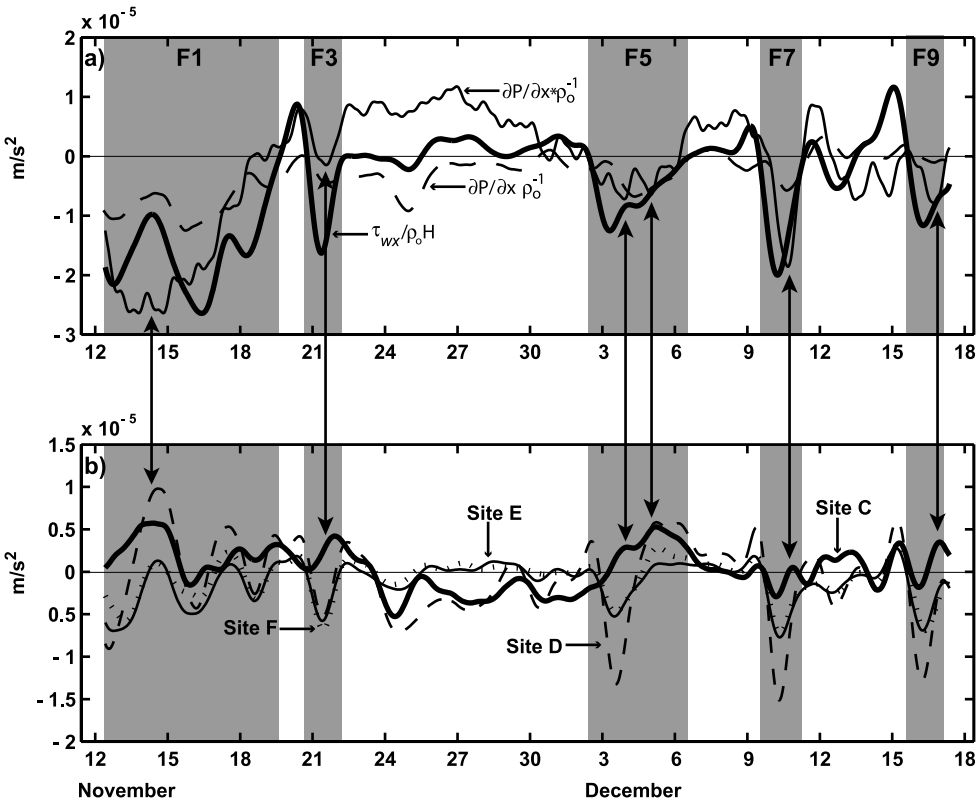

Figure 8. Comparison of the (a) alongshore bed stress to the alongshore wind stress (bold line) and alongshore pressure gradient between two sites within Long Bay (solid line) and Cape Hatteras, North Carolina, and Oyster Landing (dashed line) (b) at sites C, D, E, and F. Here $-1/\rho_o \cdot \partial P/\partial x$ was graphed without the negative signs to illustrate the similarity in magnitude with $\tau_{wx}/\rho_o H$. Arrows denote where the alongshore pressure gradient approaches the magnitude of the alongshore wind stress and coincides with periods where the alongshore velocity at site C often opposes those of the stations farther offshore.

ing favorable) in the spring and southwestward winds (downwelling favorable) in the fall. In the spring, near-bed flows at site A (nearshore) were directed predominantly alongshore with the wind while those at site B (farther offshore) were directed onshore. Examination of the full current profile at site B revealed that flows during these conditions were vertically segregated into distinct surface and bottom layers, with the flow in the surface layer being aligned with the wind to the northeast while flow in the bottom layer was directed onshore. During strong southwestward winds no vertical flow segregation was observed and flows at both stations were aligned with the wind when wind stresses exceeded $\sim$0.1 N/m^2. In the fall, spatial variations in the flow field occurred during southwestward winds. In these periods flows at sites D, E, and F were generally aligned with the wind, while flow at site C (nearshore) was either significantly smaller than the flow at the offshore sites or opposed both the wind and currents observed at the other locations. Northeastward winds in the fall occurred less often, and were weaker than those observed in the spring resulting in weaker, yet similar flows at all sites. The plausible causes for the spatial variations in near-bed flows during northeastward winds (upwelling favorable) in the spring and southwestward winds (downwelling favorable) in the fall are examined in the following two sections.

5.1. Two-Layered Flow

[33] On the basis of similarities to observations at other inner shelf environments in the Georgia Bight [*Blanton and Atkinson*, 1983] and the North Carolina shelf [*Lentz*, 2001], the two-layered flow observed in the spring must be facilitated by vertical stratification. Stratification decouples the surface and bottom layers and is observed primarily during northeastward winds (upwelling favorable), which can cause offshore transport in the surface layer that is compensated by onshore transport of more dense midshelf water at depth. On the other hand, the stratification breaks down during sufficiently strong southwestward winds (downwelling favorable) as cross-shelf flows force lighter water under heavier water enabling vertical mixing [*Austin and Lentz*, 2002]. Consequently, flows during these conditions are driven with the wind throughout the water column.

[34] While it could be argued that the observed two-layer flow is a product of Ekman-like flow, the small flow depth (12 m) makes this situation unlikely. The two-layer flow pattern was observed mainly during energetic northeastward wind events where the wind stress exceeded 0.1 N/m^2. In a

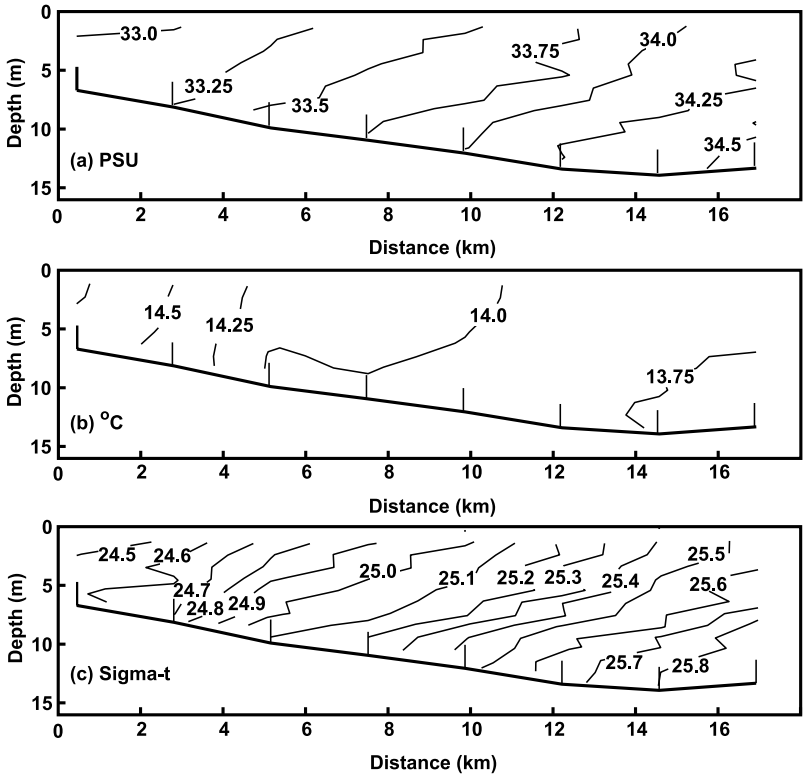

Figure 9. A cross-shore profile of (a) salinity, (b) temperature, and (c) density based on data acquired in April 2004. Vertical lines along seabed denote location of CTD casts. The transect was acquired 1 day after a period of southwesterly and westerly wind (upwelling favorable). Location of transect is noted in Figure 1.

homogeneous water column that is shallower than the Ekman depth, a wind stress of this magnitude will cause the surface and bottom boundary layers to merge so that flow throughout the water column will be aligned with the wind stress [*Lentz*, 1995]. With a vertically stratified water column, which often persists during northeastward winds [e.g., *Blanton and Atkinson*, 1983; *Lentz*, 2001; *Austin and Lentz*, 2002] however, the buoyancy forces inhibit vertical mixing keeping surface and bottom layers separated. The lack of observed two-layered flow at sites E and F (8.4 and 12.4 m, respectively) in the fall period is attributed to the fact that upwelling favorable wind events were smaller in magnitude and duration than those noted during the spring period.

[35] Temperature and salinity measurements were not available to verify the vertical density gradients facilitated the two-layered flows that occurred during northeastward winds in the spring. Instead, we conducted a rough estimate of the minimum vertical density gradient ($\Delta\rho$) required to sustain a stratified water column during the four two-layered flow events (S1, S7, S11, and S12, see Figure 5) using the bulk Richardson number, which is used to express the stability of the water column,

$$\mathrm{Ri} = \frac{\left(\frac{-g\Delta\rho}{\rho_o \Delta z}\right)}{\left(\frac{\Delta u}{\Delta z}\right)^2} \qquad (2)$$

where $\Delta\rho/\Delta z$ and $\Delta u/\Delta z$ are the density and velocity gradient between the top and bottom layers (assumed to be at 8.2 and 3.2 m above the bed), and ρ_o is a reference density (1026 kg/m^3). The term $\Delta u/\Delta z$ was determined from the data along the direction of the surface current. The minimum bulk density gradient needed to sustain stratification (i.e., for Ri = 0.25) for the flow conditions in these four cases was 0.15, 0.29, 0.38, and 0.16 kg/m^3. These $\Delta\rho$ values correspond to either differences in salinity or temperature as much as 0.5 ppt or 3°C respectively. The occurrence of such conditions on the Long Bay inner shelf is not unusual. Salinity and temperature data from CTD transects collected in April of 2004 (Figure 9) after 2 days of northeastward wind reveal vertical density differences of 0.30 kg/m^3 in the region 8–16 km from the coast. This gradient is weaker than that noted on the North Carolina shelf [*Lentz*, 2001] and in the Georgia Bight [*Lee et al.*, 1985] yet it provides a minimum estimate of the vertical density gradient needed to decouple surface and bottom layers. As such, even for portions of the SAB inner shelf with relatively limited freshwater input from coastal rivers, such as the site considered here, density gradients influence the flow response to northeastward wind conditions.

5.2. Nearshore Flow Reversal

[36] The evaluation of the alongshore momentum balance over the fall 2001 period (see section 4.4) revealed that the alongshore pressure gradient approached or exceeded the magnitude of the alongshore wind stress during southwestward winds. These cases coincided with periods where the currents at site C were either smaller than or

Table 5. Slope (m), Intercept (b), and Correlation Coefficients (r) for the Relation R = mF + b, Where F is a Forcing Term [$\tau_{wx}/\rho_o H + 1/\rho \cdot \partial P/\partial x$] and R Is a Response Term [$\tau_{bx}/\rho_o H$][a]

	m	b	r
Site C	0.13 ± 0.0002	0.0001	0.33
Site D	0.3 ± 0.0004	0	0.41
Site E	0.07 ± 0.0002	−0.0001	0.2
	0.1 ± 0.0002	*0.0001*	*0.28*
Site F	0.06 ± 0.0002	−0.0001	0.17
	0.1 ± 0.0002	*0*	*0.28*

[a]The italicized results for sites E and F were computed for R also containing the Coriolis and local accelerations: [$\tau_{bx}/\rho_o H + \partial u/\partial t - fv$] following *Lentz et al.* [1999]. None of the correlation coefficients is significantly different from zero at the 95% level.

were directed against the wind as well as against the flow at the other stations located farther offshore (see Figure 8, events F1, F3, F5, F7, and F9). In three cases, events F3, F5, and F7, the magnitude of the alongshore pressure gradient estimated within Long Bay approached that of the alongshore wind stress as the wind diminished and flows at all four locations rotated to the northeast. These observations suggests that the alongshore pressure gradient influences the flow reversal at site C and relaxation-like flow at all stations.

[37] This leads us to examine the role of the pressure gradient as a forcing or response at our study site. *Lentz et al.* [1999] parameterized the forcing [$F = \tau_{wx}/\rho_o H - 1/\rho \cdot \partial P/\partial x$] and response portions [$R = \tau_{bx}/\rho_o H + \partial u/\partial t - fv$] of the alongshore momentum balance to confirm that the estimated terms closed the momentum balance. When the same approach was attempted with our data, poor correlations and regression coefficients were achieved between these terms (Table 5). Instead, when we define wind as the only forcing [$F = \tau_{wx}/\rho_o H$] and group all remaining terms as the response [$R = 1/\rho \cdot \partial P/\partial x + \tau_{bx}/\rho_o H + \partial u/\partial t - fv$], the correlations between F and R, are much higher in this case for sites E and F (0.83 and 0.82, respectively) and the regression coefficients approach 1 (Table 6). The correlations remain almost the same if we ignore the acceleration and Coriolis terms suggesting that their role is minor as mentioned in section 4.3. Therefore the analysis is simplified assuming that the response (R) at all sites is defined by the pressure gradient and bottom stress terms [$1/\rho \cdot \partial P/\partial x + \tau_{bx}/\rho_o H$] while the forcing (F) is only the wind stress term.

[38] Comparison of the newly defined F and R functions for all four sites resulted in regressions with slopes varying from 0.8 to 1.1, with correlations coefficients ranging from 0.75 and 0.8 (significant at the 99% level). Our results suggest that the pressure gradient term was part of the response to southwestward winds (downwelling favorable) rather than part of the forcing mechanism as noted on the North Carolina shelf [*Lentz et al.*, 1999] where it was argued that larger-scale processes such as the Chesapeake Bay plume and the large-scale wind field influenced the alongshore pressure gradient.

[39] To further explore the generation of the counter flow that was especially prominent at site C during southwestward winds, the linearized depth-averaged alongshore momentum equation was integrated in time following *Lentz* [1994] and *Lentz et al.* [1999] to estimate the magnitude of the alongshore current (u_p) that should develop in response to wind stress and pressure gradient observations,

$$\overline{u}_p = \int_{t_o}^{t} \left(-\frac{1}{\rho_o}\frac{\partial P}{\partial x} + \frac{\tau_{wx}}{\rho_o h} \right) e^{-(t-t')/T_f} dt' + \overline{u}_o e^{-(t-t_o)/T_f} \qquad (3)$$

where $T_f = h/r$ is the frictional timescale, u_o is the observed alongshore current at $t = t_o$, t' represents each time step, and h is the water depth while the term r is a linear friction factor. In this study the frictional timescale was defined as a function of the bed shear stress (u_{*c}) that was estimated using the BBLM model (see section 4.3). This definition ($T_f = (h \cdot u)/u_{*c}$) was derived by equating the linear with the quadratic relationships and solving the equations below for r:

$$\begin{aligned} u_{*c}^2 &= C_D \cdot u^2 \\ u_{*c}^2 &= r \cdot u \end{aligned} \qquad (4)$$

[40] To examine the relative importance of the alongshore winds stress and the alongshore pressure gradient, the alongshore velocity (u_p) specified in equation (3) was calculated for three cases: (1) assuming that the wind stress term is zero; (2) including the values of the alongshore wind stress and pressure gradient terms as derived from the data; and (3) as the previous case with the wind stress term reduced by 50%. The predicted velocities from equation (3) are compared to the measured near-bed and depth-averaged alongshore velocities at sites C and E (Figure 10). While the near-bed velocity at site C is expected to be slightly smaller than the depth averaged velocity, it gives an indication of the current direction.

[41] The closest correspondence of the predicted velocity (u_p) to velocity observations from site C was achieved for case 3 where the alongshore wind stress was reduced by 50% (Figure 10d). Figure 10 illustrates that the observed velocity at C and u_p are nearly identical during the initial phases of event F1 and during events F7 and F9. Otherwise, the predicted velocity for this case does not match site C during the other events or site E at any time. For case 1, the predicted (u_p) and measured velocity at site C are similar during the initial portions of events F1 and F5 while the current observations from site E do not agree with u_p (Figure 10b). In case 2, the inclusion of both the observed wind stress and pressure gradient produce a u_p that agreed

Table 6. Slope (m), Intercept (b), and Correlation Coefficients (r) for the Relation R = mF + b, Where F is a Forcing Term [$\tau_{wx}/\rho_o H$] and R Is a Response Term [$1/\rho \cdot \partial P/\partial x + \tau_{bx}/\rho_o H$][a]

	m	b	r
Site C	0.8 ± 0.0006	0.0002	0.75
Site D	1.0 ± 0.0006	0.0002	0.8
Site E	1.1 ± 0.0006	0.0002	0.82
	1.1 ± 0.0006	*0.0002*	*0.83*
Site F	1.1 ± 0.0007	0.0002	0.8
	1.1 ± 0.0006	*0.0002*	*0.82*

[a]Italicized results for sites E and F were computed for R also containing the Coriolis and local accelerations: [$1/\rho \cdot \partial P/\partial x + \tau_{bx}/\rho_o H + \partial u/\partial t - fv$] following *Lentz et al.* [1999].

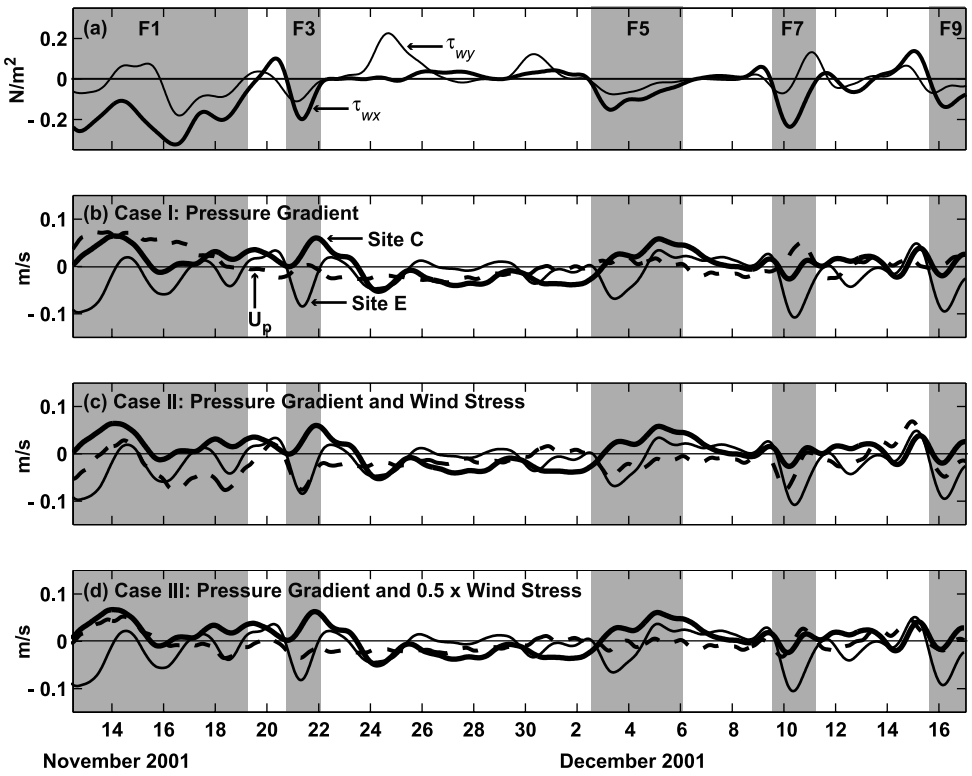

Figure 10. Time series of (a) wind stress (b) and predicted alongshore current (u_p, dashed line) estimated as a function of the pressure gradient alone, (c) the pressure gradient and the wind stress, and (d) the pressure gradient with a reduced wind stress. Alongshore current observations from sites C and E are also displayed.

more closely with the depth-averaged current that was observed at site E (Figure 10c). The correspondence between these time series was close especially during the southwestward wind events (F1, F3, F5, F7, and F9).

[42] The fact that the closest agreement between u_p and the alongshore velocity at site C occurred for case 3 suggests that the wind stress used for this approximation may be an over estimate of the alongshore wind stress close to shore. A comparison of wind observations from Springmaid Pier in 2004, which is located 12 km to the southwest of site C, to wind observations from Frying Pan Shoals for periods where the wind blew out of the southwest or northeast quadrants shows that the alongshore wind components are well correlated (R = 0.8) but are on average 20–25% less at Springmaid Pier (Figure 11). This difference results in a roughly 30–40% difference in wind stress, which approaches the value that was used to approximate the alongshore current in case 3. In this situation, the alongshore pressure gradient is a larger forcing term close to the coast where the wind stress is reduced presumably because of the influence of land. As a result the alongshore pressure gradient appears to be a dominant factor generating the nearshore flow against the wind.

[43] While the above analysis has provided some insight into the mechanisms contributing to the nearshore flow reversals at site C, it does not reproduce the relaxation-like flow reversals observed at all four sites as southwestward winds diminished toward the end of events F3, F5, and F7 (see Figure 6). This flow relaxation is similar to that observed at other sites, but for upwelling conditions [*Winant et al.*, 1987; *Send et al.*, 1987; *Chant et al.*, 2004]. Despite the inability to simulate the relaxation-like current pattern in the present study, our observations show that this flow relaxation pattern occurs when the alongshore pressure gradient approaches or exceeds the magnitude of the alongshore wind stress. This occurs as southwestward winds subside (see Figure 6, events F1, F3, and F5).

[44] An alternative idea that was pursued involved the possibility that alongshore variations in wave setup could have created localized pressure gradients that affected the alongshore current. In the absence of direct measurements, a nearshore wave model (SWAN [*Booij et al.*, 1999]) (not shown here) was used to evaluate whether or not wave setup could occur during high-wind conditions. The modeling efforts produced no evidence that wave setup occurred under the wind conditions that prevailed during the fall period. In addition, the significant wave height at site C never exceeded one third of the water depth indicating that wave breaking did not occur.

[45] An interesting aspect of this problem that could not be clearly explored because of limited measurements is the influence of the cuspate shape of Long Bay on the alongshore pressure gradient. Toward Cape Romain, located at the southwestern end of Long Bay, the coastline protrudes onto the shelf (see Figure 1 inset b) and may contribute to localized sea surface setup which could accentuate the alongshore pressure gradient during southwestward winds (downwelling favorable). The enhanced alongshore pressure gradient could be large enough at times to counter and surpass the forcing of the alongshore wind stress

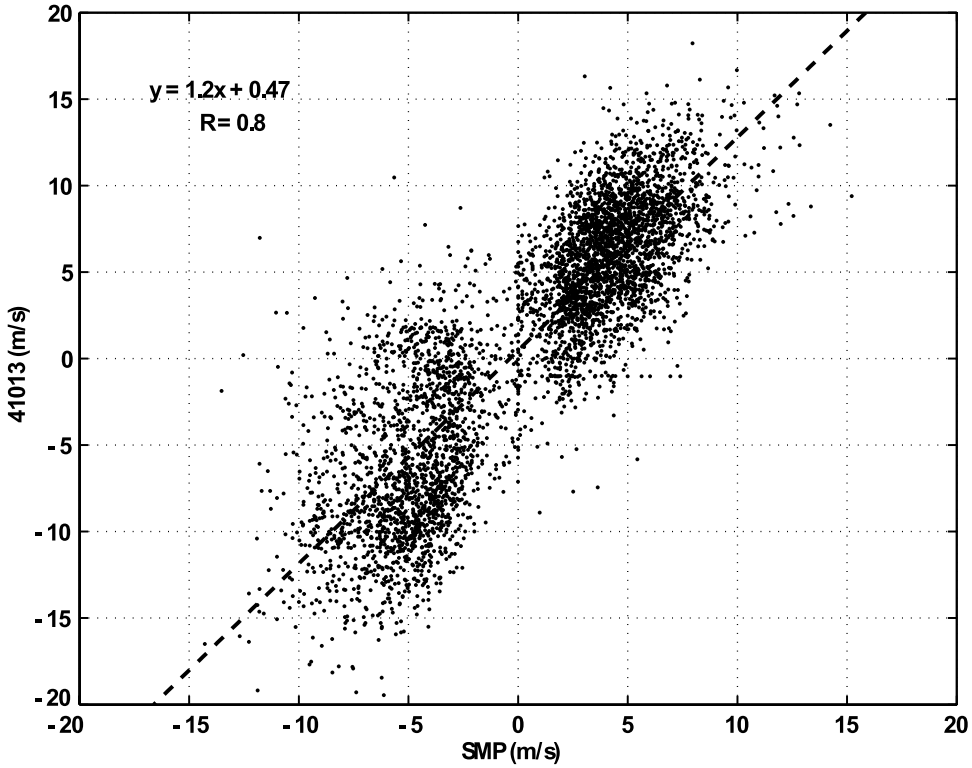

Figure 11. Scatterplot of alongshore components of wind velocity during periods where the wind directions were from the northeast and southwest quadrants. Observations were obtained from weather stations at Springmaid Pier and NOAA Buoy 41013 at Frying Pan Shoals.

causing the observed variations and reversal of the alongshore current. The coarse spacing of tidal stations along the North and South Carolina coasts made it difficult to resolve alongshore variations in the pressure gradient that could be attributed to variations in coastal morphology. Where the alongshore pressure gradient was estimated with in Long Bay and over a larger distance between Cape Hatteras and the Oyster Landing station, it showed a similar response during southwestward winds. The response within Long Bay was similar to observations at other sites where the alongshore pressure gradient was correlated to, similar in magnitude to, and opposed the alongshore wind stress [e.g., *Lentz*, 1994; *Wong*, 1999]. In these cases however, the effect of coastline morphology was not explored. In another case, *Gan and Allen* [2002a, 2002b] used a numerical model to show that alongshore variations in topography interact with wind driven coastal currents to produce pressure gradients in the vicinity of a northern California coastal cape. Their model results were in agreement with observations from the northern California continental shelf. According to *Gan and Allen*'s [2002b] work, these pressure gradients generate flow reversals in the nearshore where northward currents close to the coast oppose southward flows farther offshore when the upwelling favorable winds relax. In our study we are unable to what degree the alongshore pressure gradient is enhanced by the coastline configuration in Long Bay during southwestward winds. Another aspect that could not be explored is the role of baroclinicity, which is an important factor in generating the pressure gradient in upwelling relaxation. These two aspects will be the focus of ongoing modeling and future field efforts.

6. Conclusions

[46] Analysis of subtidal current observations acquired during the spring and fall of 2001 reveals a cross-shore varying flow pattern on the inner shelf of Long Bay, South Carolina, for northeastward (upwelling favorable) and southwestward (downwelling favorable) winds, which are a dominant current forcing mechanism in the South Atlantic Bight.

[47] During northeastward winds in the spring a two-layer flow was observed on the inner shelf at a depth of 12 m. Currents in the surface layer were aligned mainly with the prevailing wind and coast, while currents in the lower layer were directed onshore. This phenomenon is in agreement with studies that have shown that upwelling favorable winds can lead to offshore transport of lighter water from nearshore regions in the surface layer and are compensated by onshore transport of denser waters from offshore in the bottom layer.

[48] During southwestward winds in the fall, alongshore flows close to the coast were often reduced compared to or opposed flows measured farther offshore. This nearshore flow reversal occurred at times where the alongshore pressure gradient approached the strength of the alongshore wind stress. Our analysis suggests that the relative strength of the alongshore pressure gradient relative to the wind stress, which appears weaker close to shore, causes the

observed flow reversal close to the coast. While our analysis provides an explanation for this nearshore flow reversal, it does not elucidate the dynamical causes of this relaxation-like response to the termination of strong southwestward winds. Consequently, further efforts focused on simulating inner shelf flows in Long Bay should address the effects of (1) cross-shore gradients in the alongshore wind stress, (2) large-scale coastal morphology of Long Bay, and (3) inner shelf density gradients.

[49] **Acknowledgments.** Funding for this work was provided by the U.S. Geological Survey as part of the SC Coastal Erosion Study and by the South Carolina Sea Grant Consortium (Project R/CP-11). Harvey Seim is thanked for the use of his 600 kHz ADCP that was deployed at site F. Support for the first author was provided by the Department of Education GAANN program awarded to the University of South Carolina. John Warner of the U.S. Geological Survey reviewed an early version of this manuscript and provided helpful comments. Rosario Sanay also gave helpful advice regarding this manuscript. Last, we appreciate the input received from two anonymous reviewers.

References

Atkinson, L. P., and D. W. Menzel (1985), Introduction: Oceanography of the southeast United States continental shelf, in *Oceanography of the Southeastern U.S. Continental Shelf*, *Coastal Estuarine Sci.*, vol. 2, edited by L. P. Atkinson, S. W. Menzel, and K. A. Bush, pp. 1–9, AGU, Washington, D. C.

Atkinson, L. P., T. N. Lee, J. O. Blanton, and W. S. Chandler (1983), Climatology of the southeastern United States continental shelf waters, *J. Geophys. Res.*, *88*, 4705–4718.

Aubrey, D. G., and P. A. Speer (1984), A study of non-linear tidal propagation in shallow inlet/estuarine systems. part I: Observations, *Estuarine Coastal Shelf Sci.*, *21*, 185–205.

Austin, J. A., and S. J. Lentz (1999), The relationship between synoptic weather systems and meteorological forcing on the North Carolina inner shelf, *J. Geophys. Res.*, *104*, 18,159–18,185.

Austin, J. A., and S. J. Lentz (2002), The inner shelf response to upwelling and downwelling, *J. Phys. Oceanogr.*, *32*, 2171–2193.

Beardsley, R. C., R. Limeburner, and L. K. Rosenfeld (1985), Introduction to the CODE-2 moored array and large-scale data report, in *CODE-2: Moored Array and Large-Scale Data Report*, edited by R. Limeburner, *Tech. Rep. WHOI-85–35*, 234 pp., Woods Hole Oceanogr. Inst., Woods Hole, Mass.

Blanton, J. O. (1981), Ocean currents along a nearshore frontal zone on the continental shelf of the southeastern United States, *J. Phys. Oceanogr.*, *11*, 1627–1637.

Blanton, J. O., and L. P. Atkinson (1983), Transport and fate of river discharge on the continental shelf of the southeastern United States, *J. Geophys. Res.*, *88*, 4730–4738.

Boicourt, W., W. J. Wiseman, A. Valle-Levinson, and L. P. Atkinson (1998), Continental shelf of the southeastern United States and the Gulf of Mexico: In the shadow of the western boundary current, in *The Sea*, vol. 11, edited by A. R. Robinson and K. H. Brink, pp. 135–182, John Wiley, Hoboken, N. J.

Booij, N., R. C. Ris, and L. H. Holthuijsen (1999), A third-generation wave model for coastal regions: 1. Model description and validation, *J. Geophys. Res.*, *104*, 7649–7666.

Chant, R. J., S. M. Glenn, and J. T. Kohut (2004), Flow reversals during upwelling conditions on the New Jersey inner shelf, *J. Geophys. Res.*, *109*, C12S03, doi:10.1029/2003JC001941.

Chen, C., L. Zheng, and J. O. Blanton (1999), Physical processes controlling the formation, evolution, and perturbation of the low-salinity front in the inner shelf off the southeastern United States: A modeling study, *J. Geophys. Res.*, *104*, 1259–1288.

Gan, J., and J. S. Allen (2002a), A modeling study of the shelf circulation off northern California in the region of the Coastal Ocean Dynamics Experiment: 2. Simulations and comparisons with observations, *J. Geophys. Res.*, *107*(C11), 3184, doi:10.1029/2001JC001190.

Gan, J., and J. S. Allen (2002b), A modeling study of the shelf circulation off northern California in the region of the Coastal Ocean Dynamics Experiment: Response to relaxation of upwelling winds, *J. Geophys. Res.*, *107*(C9), 3123, doi:10.1029/2000JC000768.

Glenn, S. M., M. F. Crowley, D. B. Haidvogel, and Y. T. Song (1996), Underwater observatory captures coastal upwelling events off New Jersey, *Eos Trans. AGU*, *77*(25), 233, 236.

Kohut, J. T., S. M. Glenn, and R. J. Chant (2004), Seasonal current variability on the New Jersey inner shelf, *J. Geophys. Res.*, *109*, C07S07, doi:10.1029/2003JC001963.

Kundu, P. K., J. O. Blanton, and M. M. Janopaul (1981), Analysis of current observations on the Georgia shelf, *J. Phys. Oceanogr.*, *11*, 1139–1149.

Large, W. G., and S. Pond (1981), Open ocean momentum flux measurements in moderate to strong winds, *J. Phys. Oceanogr.*, *11*, 324–336.

Lee, T. N., and L. P. Atkinson (1983), Low-frequency current and temperature variability from Gulf Stream frontal eddies and atmospheric forcing along the southeast U.S. continental shelf, *J. Geophys. Res.*, *88*, 4541–4568.

Lee, T. N., V. Kourafalou, J. D. Wang, W. J. Ho, J. O. Blanton, L. P. Atkinson, and L. J. Pietrafesa (1985), Shelf circulation from Cape Canaveral to Cape Fear during winter, in *Oceanography of the Southeastern U.S. Continental Shelf*, *Coastal Estuarine Sci.*, vol. 2, edited by L. P. Atkinson, S. W. Mensel, and K. A. Bush, pp. 33–62, AGU, Washington, D. C.

Lee, T. N., E. Williams, J. Wang, and R. Evans (1989), Response of South Carolina continental shelf waters to wind and Gulf Stream forcing during the winter of 1986, *J. Geophys. Res.*, *94*, 10,715–10,754.

Lentz, S. J. (1994), Current dynamics on the northern California inner shelf, *J. Phys. Oceanogr.*, *24*, 2461–2478.

Lentz, S. J. (1995), Sensitivity of the inner-shelf circulation to the eddy-viscosity profile, *J. Phys. Oceanogr.*, *25*, 19–28.

Lentz, S. J. (2001), The influence of stratification on the wind-driven cross-shelf circulation over the North Carolina shelf, *J. Phys. Oceanogr.*, *31*, 2749–2760.

Lentz, S., R. T. Guza, S. Elgar, F. Feddersen, and T. H. C. Herbers (1999), Momentum balances on the North Carolina inner shelf, *J. Geophys. Res.*, *104*, 18,205–18,226.

McNinch, J. E., and R. A. Luettich (2000), Physical processes around a cuspate foreland: Implications to the evolution and long-term maintenance of a cape-associated shoal, *Cont. Shelf Res.*, *20*, 2367–2389.

Pietrafesa, L. J., G. S. Janowitz, and P. A. Wittman (1985), Physical oceanographic processes in the Carolina capes, in *Oceanography of the Southeastern U. S. Continental Shelf*, *Coastal Estuarine Sci.*, vol. 2, edited by L. P. Atkinson, S. W. Menzel, and K. A. Bush, pp. 23–32, AGU, Washington, D. C.

Schwing, F. B., B. J. Kjerfve, and J. E. Sneed (1983), Nearshore currents on the South Carolina continental shelf, *J. Geophys. Res.*, *88*, 4719–4729.

Send, U. R., R. C. Beardsley, and C. D. Winant (1987), Relaxation from upwelling in the Coastal Ocean Dynamics Experiment, *J. Geophys. Res.*, *92*, 1683–1698.

Styles, R., and S. M. Glenn (2000), Modeling stratified wave and current bottom boundary layers on the continental shelf, *J. Geophys. Res.*, *105*, 24,119–24,139.

Van Dolah, R. F. (2003), A regional perspective of issues and processes from the beach to the outer shelf: What do we know and where do we go?, paper presented at Southeast Coastal Ocean Science Conference and Workshop, NOAA, Charleston, S. C., 27–31 Jan.

Winant, C. D., R. C. Beardsley, and R. E. Davis (1987), Moored wind, temperature and current observations made during Coastal Ocean Dynamics Experiments 1 and 2 over the northern California continental shelf and upper slope, *J. Geophys. Res.*, *92*, 1569–1604.

Wong, K. C. (1999), The wind driven currents on the Middle Atlantic Bight inner shelf, *Cont. Shelf Res.*, *19*, 757–773.

B. T. Gutierrez, Department of Geological Sciences, University of South Carolina, Columbia, SC 29208, USA. (bgutierrez@usgs.gov)

G. Voulgaris, Marine Science Program, University of South Carolina, Columbia, SC 29208, USA.

P. A. Work, School of Civil and Environmental Engineering, Georgia Institute of Technology, Savannah, GA 31407, USA.